Acta Biomaterialia xxx (2014) xxx–xxx

Contents lists available at ScienceDirect

Acta Biomaterialia

journal homepage: www.elsevier.com/locate/actabiomat

Thermomechanical properties of Ni–Ti shape memory wires containing nanoscale precipitates induced by stress-assisted ageing

D.Y. Cong [a,b,*], G. Saha [a], M.R. Barnett [a]

[a] Institute for Frontier Materials, Deakin University, 75 Pigdons Road, Waurn Ponds, VIC 3216, Australia
[b] State Key Laboratory for Advanced Metals and Materials, University of Science and Technology Beijing, No. 30 Xueyuan Rd, Haidian District, Beijing 100083, People's Republic of China

ARTICLE INFO

Article history:
Received 3 June 2014
Received in revised form 9 August 2014
Accepted 18 August 2014
Available online xxxx

Keywords:
Shape memory alloys
Precipitates
Thermomechanical properties
Twin boundary movement
Phase transformation

ABSTRACT

This paper systematically examines the thermomechanical properties and phase transformation behaviour of slightly Ni-rich Ni–Ti biomedical shape memory wires containing homogeneously distributed nanoscale precipitates induced by stress-assisted ageing. In contrast to previous studies, particular attention is paid to the role of precipitates in impeding twin boundary movement (TBM) and its underlying mechanisms. The size and volume fraction of precipitates are altered by changing the ageing time. The martensitic transformation temperatures increase with prolonged ageing time, whereas the R-phase transformation temperature remains relatively unchanged. The stress–strain behaviour in different phase regions during both cooling and heating is comprehensively examined, and the underlying mechanisms for the temperature- and thermal-history-dependent behaviour are elucidated with the help of the established stress–temperature phase diagram. The effect of precipitates on TBM is explored by mechanical testing at 133 K. It is revealed that the critical stress for TBM (σ_{cr}) increases with increasing ageing time. There is a considerable increase of 104 MPa in σ_{cr} in the sample aged at 773 K for 120 min under 70 MPa compared with the solution-treated sample, owing to the presence of precipitates. The Orowan strengthening model of twinning dislocations is insufficient to account for this increase in σ_{cr}. The back stress generation is the predominant mechanism for the interactions between precipitates and twin boundaries during TBM that give rise to the increase in σ_{cr}. Such results provide new insights into the thermomechanical properties of precipitate containing Ni–Ti biomedical shape memory wires, which are instructive for developing high-performance biomedical shape memory alloys.

1. Introduction

Shape memory alloys (SMAs) possess the unique characteristics of shape memory effect and superelasticity, as a result of temperature- or stress-induced martensitic transformation [1–12], proving to be quite attractive functional materials. At present, near-equiatomic Ni–Ti alloys are the best performing and the most widely used SMAs in commercial applications [13], especially in biomedical fields [14], because they combine excellent functional performance with superb mechanical properties [1,6], superior corrosion resistance [15] and good biocompatibility [16]. Ni–Ti SMAs are capable of recovering up to 8% strain in the form of shape memory or superelasticity [6,9]. The unique properties of shape memory and superelasticity of Ni–Ti SMAs have been broadly used in the design of medical devices in cardiology, interventional radiology and orthopaedics [17,18]. One typical example is the self-deploying endovascular stents made of Ni–Ti SMAs [18,19].

It is well recognized that coherent precipitates in SMAs play an important role in strengthening both austenite and martensite by inhibiting dislocation slip [1], thus improving the shape memory effect and superelasticity by reducing the irreversible strain resulting from permanent plastic deformation. It has also been shown that precipitate containing SMAs demonstrate superior resistance to cyclic degradation effects [20–22], which is important for enhancing the stability of functional performances in biomedical applications. Inspired by these merits, increasing efforts have been devoted to the investigation of precipitation in biomedical SMAs [12,21,23].

Ageing following solution treatment has been shown to be effective in producing fine Ni_4Ti_3 coherent precipitates in Ni-rich Ni–Ti SMAs [21]. However, for slightly Ni-rich Ni–Ti alloys (e.g. $Ni_{50.7}Ti_{49.3}$, at.%) that have martensitic transformation temperatures

* Corresponding author at: Institute for Frontier Materials, Deakin University, 75 Pigdons Road, Waurn Ponds, VIC 3216, Australia and State Key Laboratory for Advanced Metals and Materials, University of Science and Technology Beijing, No. 30 Xueyuan Rd, Haidian District, Beijing 100083, People's Republic of China.
E-mail address: congdaoyong@yahoo.com (D.Y. Cong).

http://dx.doi.org/10.1016/j.actbio.2014.08.017
1742-7061/

near ambient temperature and are thus most suitable for superelastic biomedical applications, conventional ageing is not sufficient to generate homogeneously distributed precipitates [24]. Instead, it leads to a heterogeneous microstructure with precipitates predominately nucleated near grain boundaries [24]. This is because the nucleation energy barrier for the formation of Ni_4Ti_3 in B2 austenite is high, and heterogeneous nucleation at grain boundaries is energetically favourable [25,26]. This type of heterogeneous microstructure can be detrimental for practical applications. Fortunately, the novel treatment of stress-assisted ageing (ageing under bias stress) has been proved to be effective in producing homogeneously distributed Ni_4Ti_3 precipitates in slightly Ni-rich Ni–Ti SMAs [24,27].

So far, there have been extensive investigations on the phase transformation behaviour of precipitate-containing Ni–Ti alloys [23–29]. Multiple-step transformations during both cooling and heating have been identified [24–26,28,29] and interpreted in terms of heterogeneous microstructure with precipitates near grain boundaries and precipitate-free regions in grain interiors as a result of conventional ageing [26]. The influence of precipitates on functional properties of Ni–Ti alloys has also been studied [30,31]. Superior shape memory effect [30] and superelasticity [31] were achieved in alloys with a high density of fine precipitates. Nevertheless, the thermomechanical behaviour of the Ni–Ti alloys containing homogeneous fine precipitates, especially those induced by stress-assisted ageing, is still not well understood. In particular, little is known on the effect of precipitates on twin boundary movement in SMAs and the underlying mechanism for such effect remains undisclosed. Clarification of these issues is not only of great fundamental significance, but also of practical interest for designing high-performance biomedical SMAs.

In the present study, homogeneously distributed nanoscale precipitates are developed in slightly Ni-rich Ni–Ti biomedical shape memory wires by stress-assisted ageing. The thermal-history- and temperature-dependent mechanical behaviour, as well as its microscopic mechanisms, of these precipitate-containing samples is systematically studied. The effect of precipitates on twin boundary movement in these Ni–Ti wires is investigated. The underlying mechanism responsible for the interactions between precipitates and twin boundaries during twin boundary movement is elucidated. Such results provide new insights into the thermomechanical properties of Ni–Ti alloys with fine precipitates induced by stress-assisted ageing, which are instructive for developing novel biomedical SMAs.

2. Experimental

As Ni–Ti alloys are produced and used mostly in the form of wire, Ni-rich Ni–Ti wires were employed in this study. The wires, 100 μm in diameter with 55.8 wt.% Ni content (corresponding to $Ni_{50.73}Ti_{49.27}$ (at.%)), were purchased from Nitinol Devices and Components. The wires were received in "straight annealed" condition; this means that, after cold drawing, they were annealed in the range 773–823 K for a short time while constrained by clamping for shape setting [32].

The as-received wires were solution treated at 1073 K for 20 min, followed by water quenching. Then, some of the wires were aged at 773 K for different time periods under a constant tensile stress of 70 MPa to develop homogeneously distributed precipitates. These stress-assisted ageing experiments were performed in the dynamic mechanical analyser (DMA) from TA Instruments (DMA Q800), which enables mechanical testing from 133 to 873 K.

The thermomechanical behaviour of the aged samples, including the stress–strain behaviour at different temperatures and the temperature dependence of strain under a constant tensile stress, were studied in situ in DMA directly after the samples were aged. The microstructure of the aged samples, with particular attention to the morphology and distribution of the precipitates, was examined using high-resolution field emission scanning electron microscopy (FE-SEM) (Zeiss Supra 55VP). The precipitates were observed with the angle selective backscatter (AsB) detector at an accelerating voltage of 10 kV and a working distance of 3.5 mm. The phase transformation temperatures were determined by differential scanning calorimetry (DSC) (TA DSC Q200) in the temperature range 180–400 K, with a heating and cooling rate of 10 K min^{-1}.

3. Results and analysis

3.1. Precipitates developed by stress-assisted ageing

SEM observations revealed nanoscale precipitates in the samples aged under a constant tensile stress. To demonstrate the general distribution of such precipitates, a relatively low-magnification SEM image acquired with the AsB detector (SEM-AsB image) from the sample aged at 773 K for 120 min under 70 MPa is illustrated in Fig. 1. A high density of Ni_4Ti_3 precipitates, which are homogeneously distributed, can be observed. As revealed by earlier transmission electron microscopy studies (e.g. [26]), these Ni_4Ti_3 precipitates have a lenticular, disc-like shape.

In order to study the correlation between size and volume fraction of precipitates and ageing time, SEM-AsB images were taken from the samples aged at 773 K under 70 MPa for different time periods, as shown in Fig. 2a–c. When aged for a short time of 10 min, the sample shows fine precipitates with diameter <50 nm (Fig. 2a). With prolonged ageing time, the size of the precipitates increases. The diameter of the precipitates in the sample aged for 120 min reaches up to 300 nm (Fig. 2c). The volume fraction of precipitates was estimated using the line intersection method [26,33], and it is shown in Fig. 2d as a function of ageing time (measurements on at least five different images for each ageing condition were performed, and the mean value with the standard deviation is demonstrated in Fig. 2d). One can see that the volume fraction of precipitates increases rapidly with increasing ageing time up to 30 min, and then increases relatively slowly as ageing time increases to 120 min. This is generally consistent with the results from phase field simulation based on the diffusional process of precipitate coarsening [34].

3.2. Phase transformations

The DSC curve of the sample solution treated at 1073 K for 20 min is illustrated in Fig. 3. One can see that the solution-treated sample shows a single-step transformation, which is typical for unaged and precipitate-free NiTi alloys [35]. There is an exothermic

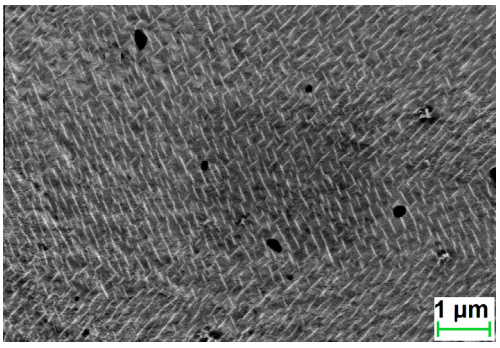

Fig. 1. Low-magnification SEM-AsB image showing the homogeneously distributed precipitates in the sample aged at 773 K for 120 min under 70 MPa.

Please cite this article in press as: Cong DY et al. Thermomechanical properties of Ni–Ti shape memory wires containing nanoscale precipitates induced by stress-assisted ageing. Acta Biomater (2014), http://dx.doi.org/10.1016/j.actbio.2014.08.017

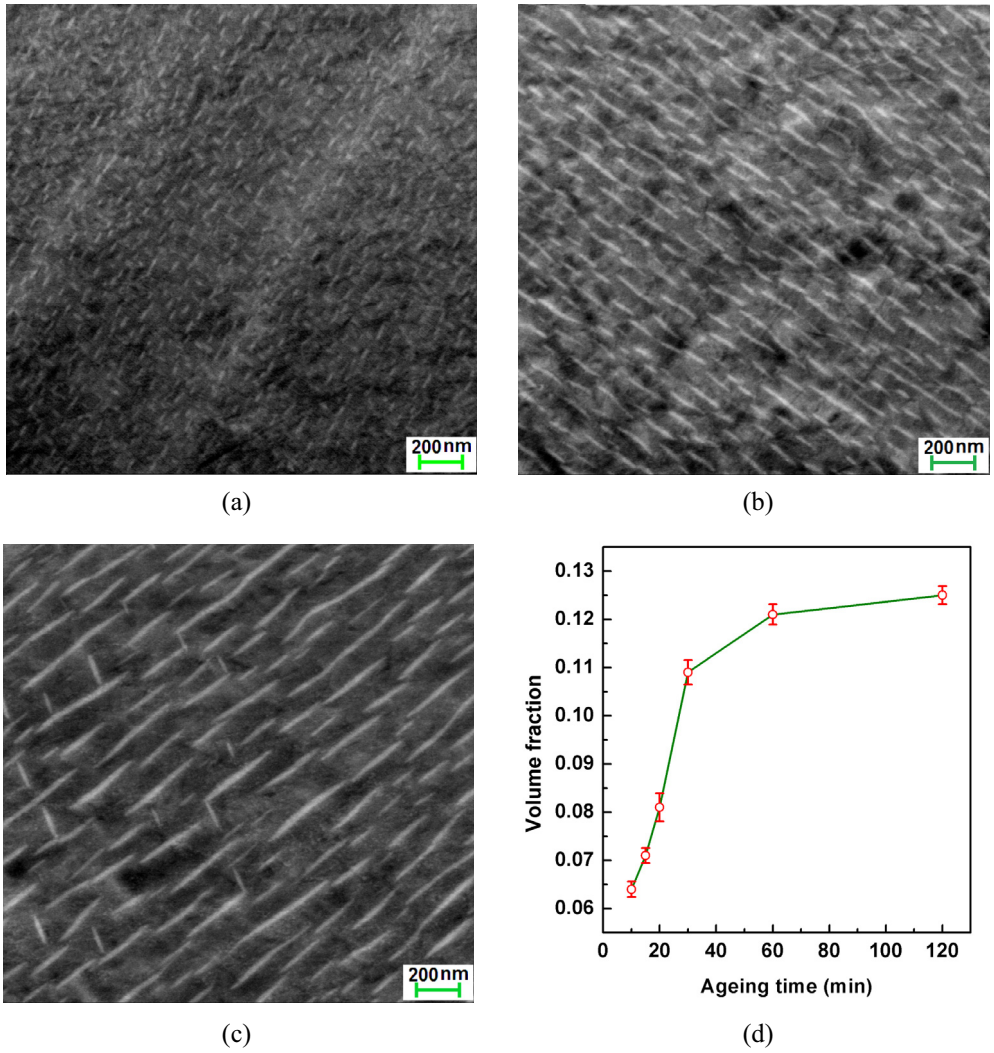

Fig. 2. (a–c) SEM-AsB images showing precipitates in samples aged at 773 K under 70 MPa for (a) 10 min, (b) 30 min and (c) 120 min. These images were taken on a cross section of the wires. (d) Volume fraction of precipitates as a function of ageing time.

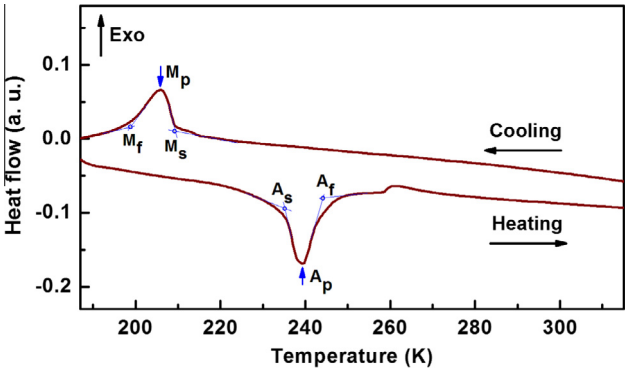

Fig. 3. DSC curve of the solution-treated sample. The determination of the transformation temperatures (M_s, M_p, M_f, A_s, A_f and A_p) is illustrated in the figure.

peak during cooling, corresponding to the martensitic transformation (from B2 austenite to B19′ martensite) and an endothermic peak during heating, corresponding to the austenitic (reverse) transformation (from B19′ martensite to B2 austenite). The martensitic transformation start, finish and peak temperatures (M_s, M_f and M_p) and the austenitic transformation start, finish and peak temperatures (A_s, A_f and A_p) are 210, 199, 206, 235, 244 and 239 K, respectively, which are determined as illustrated in Fig. 3.

A representative DSC curve for the aged samples, which is obtained from the sample aged at 773 K for 120 min under 70 MPa, is shown in Fig. 4a. Clearly, the aged samples show two-step transformations during cooling and a single-step transformation during heating. It should be noted that there are two low-temperature phases in the aged samples: R phase and B19′ phase [24], both are martensitic in nature; however, to differentiate, when "martensite" is mentioned it refers uniquely to the B19′ phase throughout this paper. The first exothermic peak during cooling (Fig. 4a) corresponds to the R-phase transformation from B2 austenite to R phase, and the second corresponds to the martensitic transformation from R phase to B19′ martensite (this martensitic transformation is different from that in the solution-treated sample, which is directly from B2 austenite to B19′ martensite). The endothermic peak during heating (Fig. 4a) corresponds to the austenitic transformation from B19′ martensite to B2 austenite. The determination of the R-phase transformation peak temperature R_p, as well as M_p and A_p, is illustrated in Fig. 4a. For comparison, the cooling and heating parts of the DSC curves of the samples aged for different time periods are demonstrated in Fig. 4b and c, respectively (the curve of the solution-treated sample is also included for reference).

Please cite this article in press as: Cong DY et al. Thermomechanical properties of Ni–Ti shape memory wires containing nanoscale precipitates induced by stress-assisted ageing. Acta Biomater (2014), http://dx.doi.org/10.1016/j.actbio.2014.08.017

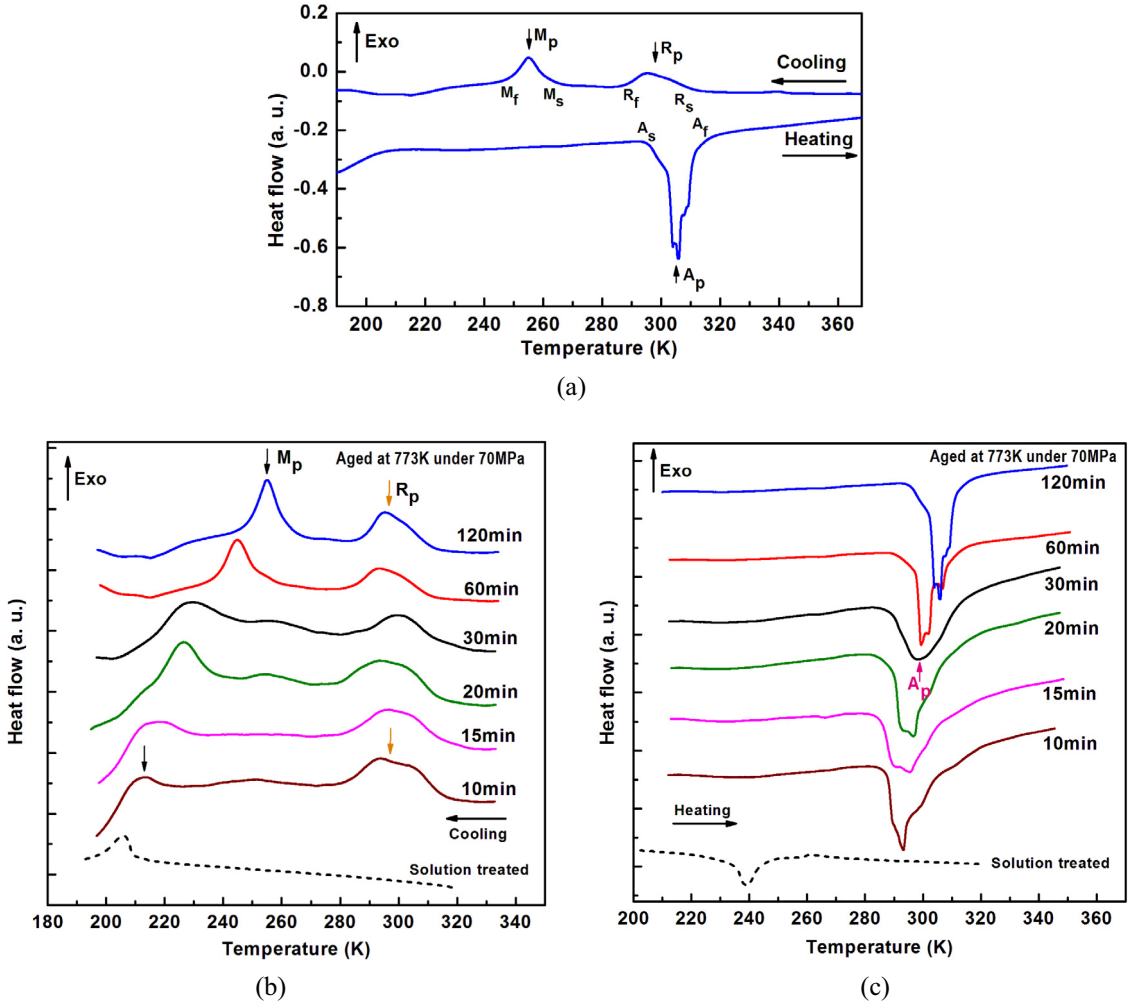

Fig. 4. (a) DSC curve of the sample aged at 773 K for 120 min under 70 MPa. The determination of the transformation temperatures R_p, M_p and A_p is illustrated. (b) Cooling and (c) heating parts of DSC curves of the samples aged at 773 K under 70 MPa for 10, 15, 20, 30, 60 and 120 min. The DSC curve of the solution-treated sample (dashed curve) is also included in (b) and (c) for reference.

The stress field introduced by coherent precipitation accounts for the two-step transformations during cooling in the samples subjected to stress-assisted ageing. It was reported that the Ni–Ti samples with coherent Ni_4Ti_3 precipitates show R-phase transformation, whereas those with incoherent precipitates do not [36]. This is because the coherency stress field resulting from coherent precipitation induces additional energy that consequently affects the relative stability of R phase and B19′ martensite [6], leading to the formation of R phase before the subsequent transformation to B19′ martensite. The fact that the sample aged at 773 K for 120 min under 70 MPa still shows R-phase transformation indicates that the relatively coarse precipitates (Fig. 2c) in that sample are still coherent.

The transformation temperatures R_p, M_p and A_p of the samples subjected to stress-assisted ageing (determined from Fig. 4b and c) are shown as a function of ageing time in Fig. 5. As shown in Figs. 4b and 5, M_p increases monotonically as the ageing time increases from 10 min to 120 min. In contrast, R_p does not depend strongly on ageing time, and keeps a value of around room temperature for all the aged samples. Consequently, the temperature range where the R phase is stable becomes narrower as the ageing time increases (Fig. 4b). Showing a trend similar to M_p, A_p also increases monotonically with prolonged ageing time, from 293 K for the sample aged for 10 min to 306 K for the sample aged for 120 min, as shown in Figs. 4c and 5. The possible mechanisms for the effect of ageing on phase transformation temperatures have been considered elsewhere [24–26] and are discussed further in Section 4.2.

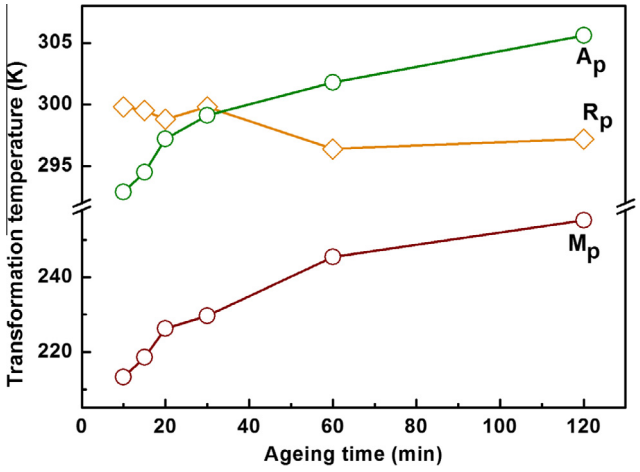

Fig. 5. Dependence of transformation temperatures R_p, M_p and A_p on ageing time.

Please cite this article in press as: Cong DY et al. Thermomechanical properties of Ni–Ti shape memory wires containing nanoscale precipitates induced by stress-assisted ageing. Acta Biomater (2014), http://dx.doi.org/10.1016/j.actbio.2014.08.017

3.3. Thermomechanical properties

3.3.1. Solution-treated sample

The stress–strain curves of the solution-treated sample measured at various temperatures are shown as solid lines in Fig. 6a–d. For these measurements, one sample is used only for one test at a certain temperature, to avoid the possible effect of permanent plastic deformation during the previous test, as would be the case if one sample was used for multiple tests at different temperatures (hereafter, "permanent plastic deformation" refers uniquely to the plastic deformation by dislocation slip, which is not recoverable either on unloading or on heating). For each measurement, the sample was first cooled or heated to the target temperature from room temperature, then the stress–strain behaviour was tested and, finally, the sample was heated to 373 K (above A_f) to examine the recovery of the residual strain (after unloading) during heating (as shown by the dashed arrows in Fig. 6b–d).

It is interesting to see that the stress–strain curves over a wide temperature range of 253–153 K (Fig. 6b–d) appear similar in shape, despite the different phases expected to be present at each testing temperature. Fig. 6e shows the strain–temperature curve under a constant tensile stress of 70 MPa. The approximate phase transformation temperatures determined from this curve are indicated in the figure. These temperatures are largely in agreement with those determined from the DSC curve (Fig. 3). The phases at the temperatures corresponding to Fig. 6a–d can be determined from Fig. 6e: austenite at 323 and 253 K, coexistence of austenite and martensite at 213 K, and martensite at 153 K.

As seen from Fig. 6a, the sample shows typical elastic and permanent plastic deformation behaviour of austenite at 323 K. No residual strain recovers on heating to 373 K. At this temperature, stress-induced martensitic transformation (SIMT) is not possible, as it is too far away from the M_s temperature. The stress–strain curve at 253 K (Fig. 6b) shows a plateau at ~500 MPa, which is a signature for SIMT. However, this SIMT is irreversible, and the residual strain after unloading only partly recovers during heating to 373 K, as shown by the dashed arrow in Fig. 6b. This can be attributed to the plastic deformation by slip during SIMT and the stabilization of martensite by dislocation strain fields [21,37–39], considering the low yield strength of the solution-treated sample and the high critical stress for SIMT at this temperature. The stabilized martensite does not transform back to austenite on unloading, and thus the SIMT is irreversible. However, the stabilized martensite may transform back to austenite on heating, which results in the partial recovery of the residual strain; the permanent plastic deformation accounts for the unrecoverable part of the residual strain.

At 213 K, the stress–strain curve (Fig. 6c) also shows a stress plateau at ~360 MPa. During unloading, the strain remains almost unrecoverable. Upon heating, most of the residual strain recovers, but a small amount of unrecoverable strain still remains. Considering the coexistence of austenite and martensite, both SIMT and

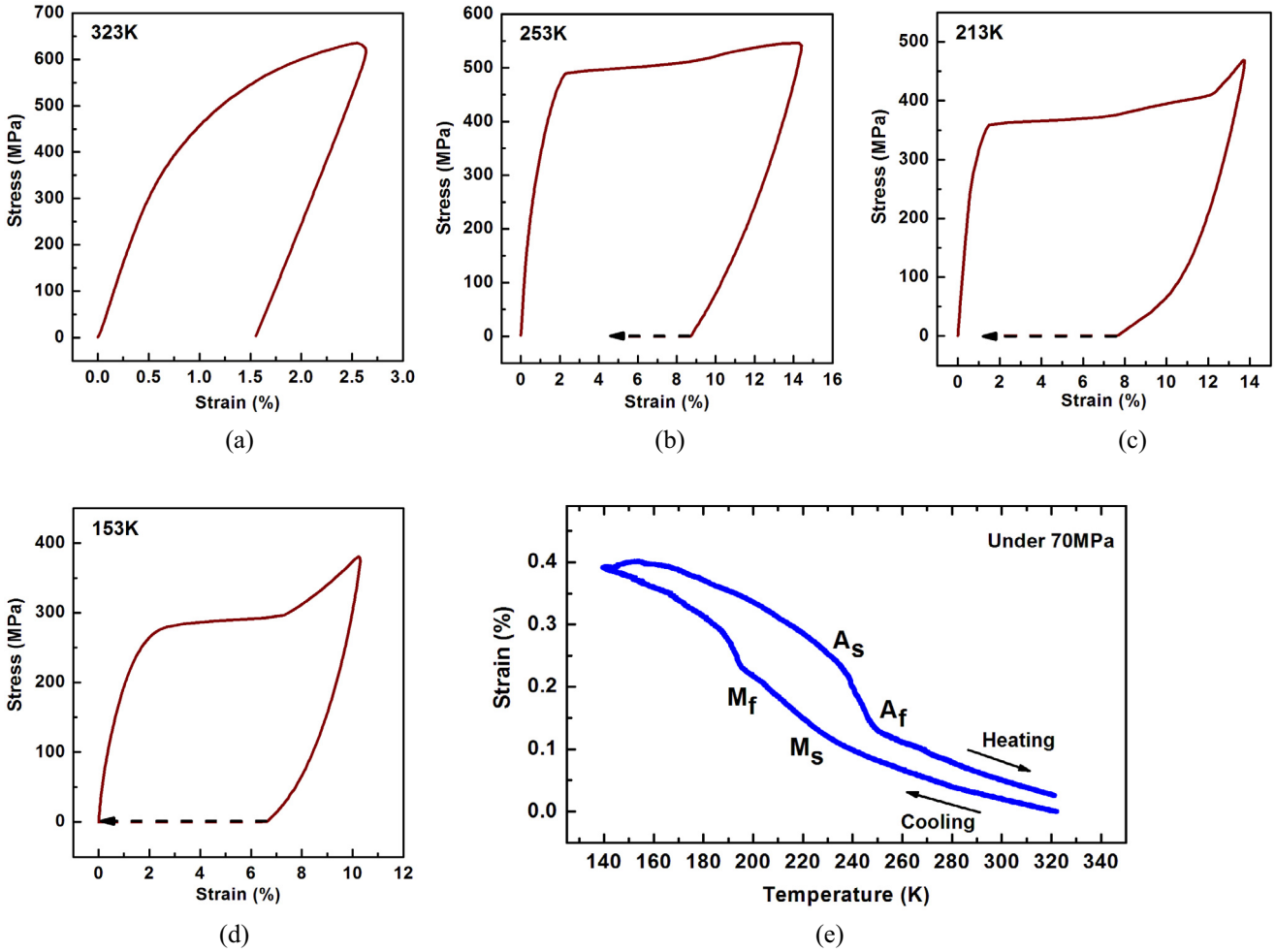

Fig. 6. (a–d) Tensile stress–strain curves (solid lines) of the solution-treated sample measured at (a) 323 K, (b) 253 K, (c) 213 K and (d) 153 K. The dashed arrows indicate the recovery of residual strain during heating to 373 K. (e) Strain–temperature curve of the solution-treated sample measured under a tensile stress of 70 MPa.

Please cite this article in press as: Cong DY et al. Thermomechanical properties of Ni–Ti shape memory wires containing nanoscale precipitates induced by stress-assisted ageing. Acta Biomater (2014), http://dx.doi.org/10.1016/j.actbio.2014.08.017

martensite reorientation via twin boundary movement occur at this temperature. The stress plateau at ~360 MPa quite probably corresponds to the SIMT, while the martensite reorientation that is likely to occur at lower stresses does not manifest itself as an obvious stress plateau owing to the constraints from the coexisting austenite. As the critical stress for SIMT is lower at this temperature (compared with the case in Fig. 6b), it is reasonable to expect less permanent plastic deformation during SIMT and, consequently, less martensite stabilized by dislocation strain fields. Nevertheless, the permanent plastic deformation cannot be excluded, because there is a small amount of unrecoverable residual strain after heating. It should be noted that, unlike the case in Fig. 6b, the martensite that is stress-induced from austenite at 213 K ($<A_s$) (Fig. 6c) is thermodynamically stable (reasonably assuming that the solution-treated sample does not precipitate at the test temperature and within the experimental time scale) after unloading, as indicated from the heating branch of the strain–temperature curve (Fig. 6e) (during unloading, the stress-induced martensite tends to transform back to austenite, and therefore the heating branch of the strain–temperature curve, which is related to the transformation from martensite to austenite, should be referred to when discussing the unloading process). The martensite reorientation is an irreversible process, the stress-induced martensite is thermodynamically stable and does not transform back; consequently, the strain is unrecoverable after unloading. Upon heating, both the reoriented martensite and the thermodynamically stable stress-induced martensite transform to austenite, which leads to the recovery of most of the residual strain; the permanent plastic deformation accounts for the small amount of unrecoverable residual strain upon heating.

At 153 K, the sample is in the pure martensitic state; the stress plateau (at ~280 MPa) on the stress–strain curve (Fig. 6d) corresponds to the martensite reorientation. Upon heating, the residual strain fully recovers, with the reoriented martensite transforming to austenite. No permanent plastic deformation can be detected from Fig. 6d, as only a relatively low critical stress is needed for martensite reorientation at this temperature.

3.3.2. Samples subjected to stress-assisted ageing

The systematic investigation performed by the present authors shows that all the samples subjected to stress-assisted ageing exhibit similar stress–strain behaviour in their respective corresponding phase regions. The only difference lies in their phase transformation temperatures. For ease of presentation, the sample aged at 773 K for 30 min under 70 MPa is selected as representative in this section.

As the stress–strain curves of the samples subjected to stress-assisted ageing have complicated features, it is difficult to elucidate the underlying mechanisms for the stress–strain behaviour without knowing the phases present during the mechanical tests. Therefore, firstly strain–temperature curves under different stresses were measured to disclose the phases at different temperatures and under different stress levels. Fig. 7 shows the strain–temperature curves measured under 70, 150, 250, 350 and 450 MPa, respectively. For each measurement, the sample was first heated to a temperature $T_1 > A_f^\sigma$ (the A_f temperature under stress σ), then a stress σ was applied, and the strain was recorded during cooling from T_1 to $T_2 < M_f^\sigma$ (the M_f temperature under σ) and during subsequent heating from T_2 to T_1; at the end of the test, the stress was released at T_1.

One can see from Fig. 7 that the sample shows perfect shape memory effect under stress levels <250 MPa, whereas degradation of the shape memory effect (manifested by unrecoverable strain) occurs under stress levels >350 MPa, because some permanent plastic deformation occurs under such high stresses. Interestingly, during cooling, the sample shows two-step transformations

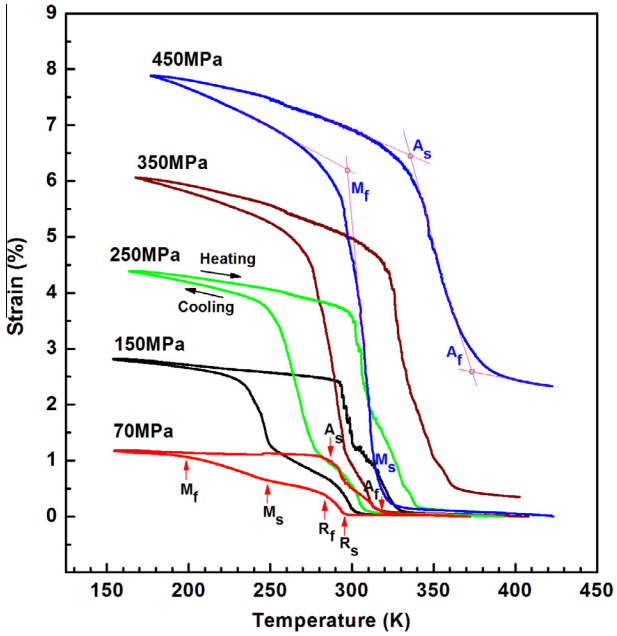

Fig. 7. Strain–temperature curves of the sample aged at 773 K for 30 min under 70 MPa, measured under a constant tensile stress of 70, 150, 250, 350 and 450 MPa, respectively. The determination of the transformation temperatures is illustrated on the curve measured under 450 MPa.

(austenite to R phase to martensite) under stresses <350 MPa, whereas it only shows a single-step transformation directly from austenite to martensite under stresses of 450 MPa (Fig. 7) and 550 MPa (not shown owing to space constraints), respectively. During heating, the sample shows a single-step transformation from martensite to austenite under all stress levels. The phase transformation temperatures under different stresses can be determined from the strain–temperature curves in Fig. 7, as demonstrated on the curve measured under 450 MPa.

Based on the transformation temperatures determined from Fig. 7, the stress–temperature phase diagram is established, which is shown in Fig. 8. This phase diagram clearly illustrates the phases under different stresses and at different temperatures both during cooling and during heating; this will be used to help interpret the stress–strain behaviour shown later. It is clear from Fig. 8 that all the phase transformation temperatures increase monotonically as the applied stress increases. However, the increase in R_s and R_f occurs more slowly than that in M_s and M_f. As a result, M_s becomes higher than R_s above a certain critical stress level and R phase transformation disappears. This is the reason why there is only a single-step transformation during cooling under high stress levels. Based on the linear fittings of the experimental data, the $d\sigma/dT$ values for R_s, R_f, M_s, M_f, A_s and A_f are determined as 18.5, 11.0, 5.4, 4.6, 7.3 and 6.0 MPa K^{-1}, respectively, which are typical values for Ni–Ti alloys [37]. The $d\sigma/dT$ values for R-phase transformation temperatures are higher than those for martensitic transformation temperatures, which is probably due to the smaller transformation strain of the R-phase transformation (~1% [6]) compared with that of the martensitic transformation (~10% [6]).

To gain a comprehensive understanding of the thermomechanical properties of the samples subjected to stress-assisted ageing, the stress–strain behaviour at different temperatures, covering a wide temperature range from above A_f to below M_f, during both cooling and heating (taking into consideration the different transformation paths during cooling and during heating) was investigated in detail. Figs. 9 and 10 demonstrate the stress–strain curves at various temperatures reached during cooling and during

Please cite this article in press as: Cong DY et al. Thermomechanical properties of Ni–Ti shape memory wires containing nanoscale precipitates induced by stress-assisted ageing. Acta Biomater (2014), http://dx.doi.org/10.1016/j.actbio.2014.08.017

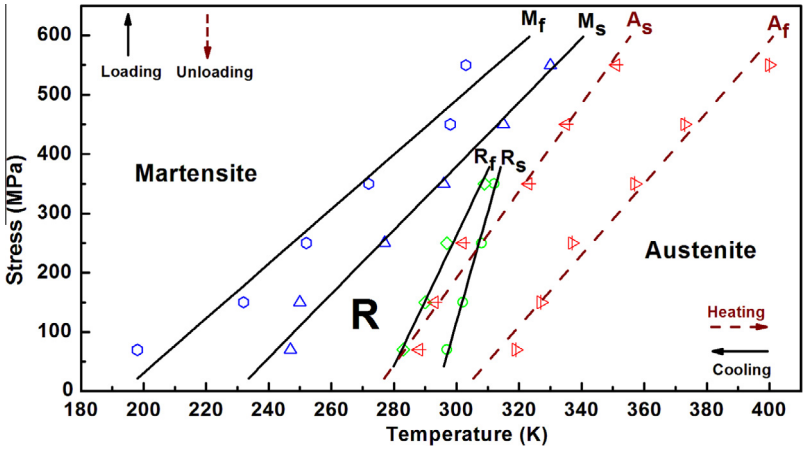

Fig. 8. Stress–temperature phase diagram for the sample aged at 773 K for 30 min under 70 MPa. The symbols denote the experimental data, and the lines are the linear fittings of the experimental data. The letter "R" in the diagram denotes the R phase.

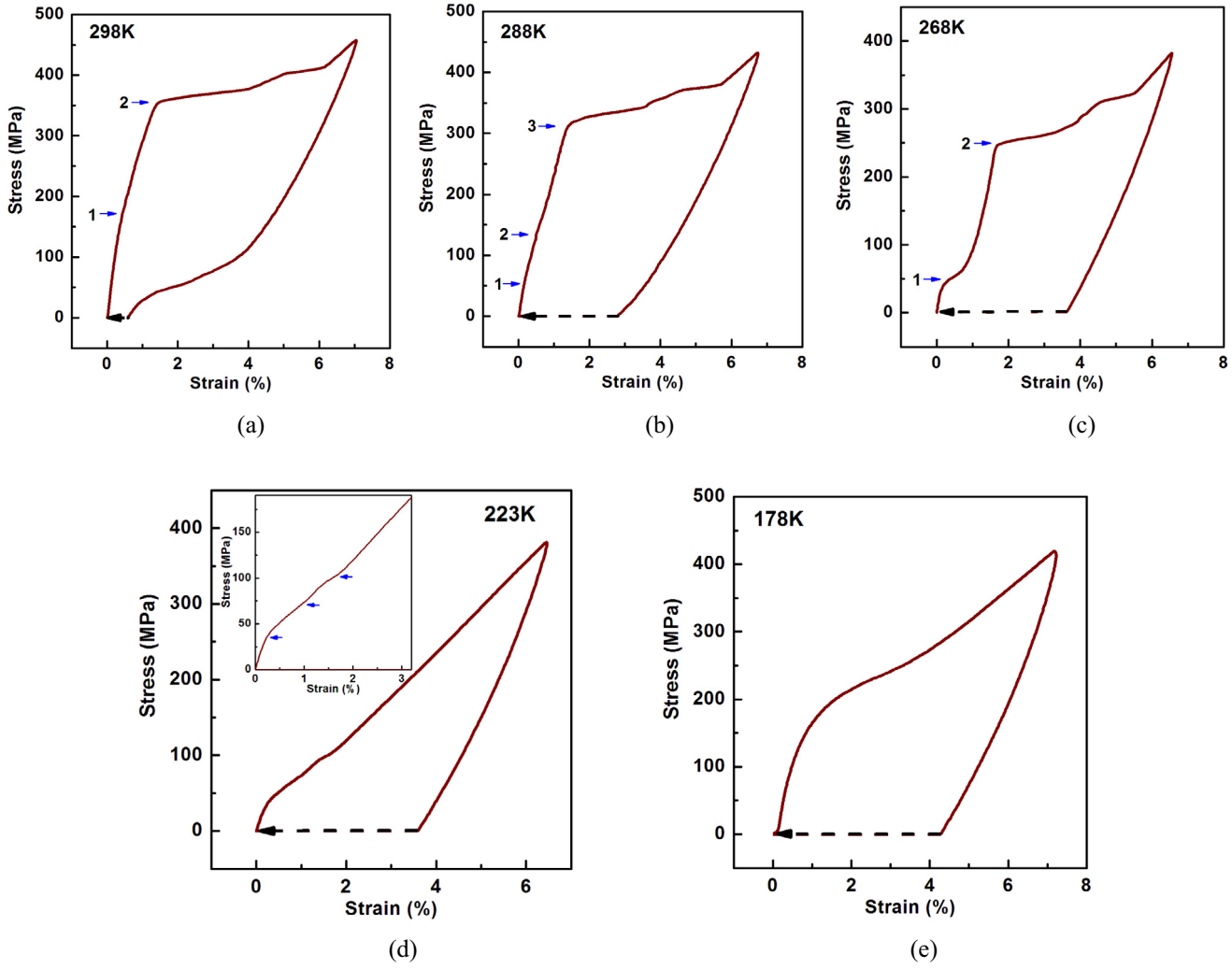

Fig. 9. Tensile stress–strain curves (solid lines) of the sample aged at 773 K for 30 min under 70 MPa, measured during cooling at (a) 298 K, (b) 288 K, (c) 268 K, (d) 223 K and (e) 178 K. The dashed arrows indicate the recovery of residual strain during heating to 393 K. The inset in (d) shows the magnified view of the stress–strain curve at low stresses during loading at 223 K.

heating, respectively. Only one sample was used for all the tests, as no permanent plastic deformation occurred prior to each test (as presented below). For the tests during cooling (Fig. 9), the sample was heated to 393 K before the first test; then the sample was cooled to the target temperature for testing, and, finally, the sample was heated back to 393 K (above A_f) to examine the recovery of the residual strain during heating (shown by the dashed arrows in Fig. 9). This cycle was repeated for all the subsequent tests. This

Please cite this article in press as: Cong DY et al. Thermomechanical properties of Ni–Ti shape memory wires containing nanoscale precipitates induced by stress-assisted ageing. Acta Biomater (2014), http://dx.doi.org/10.1016/j.actbio.2014.08.017

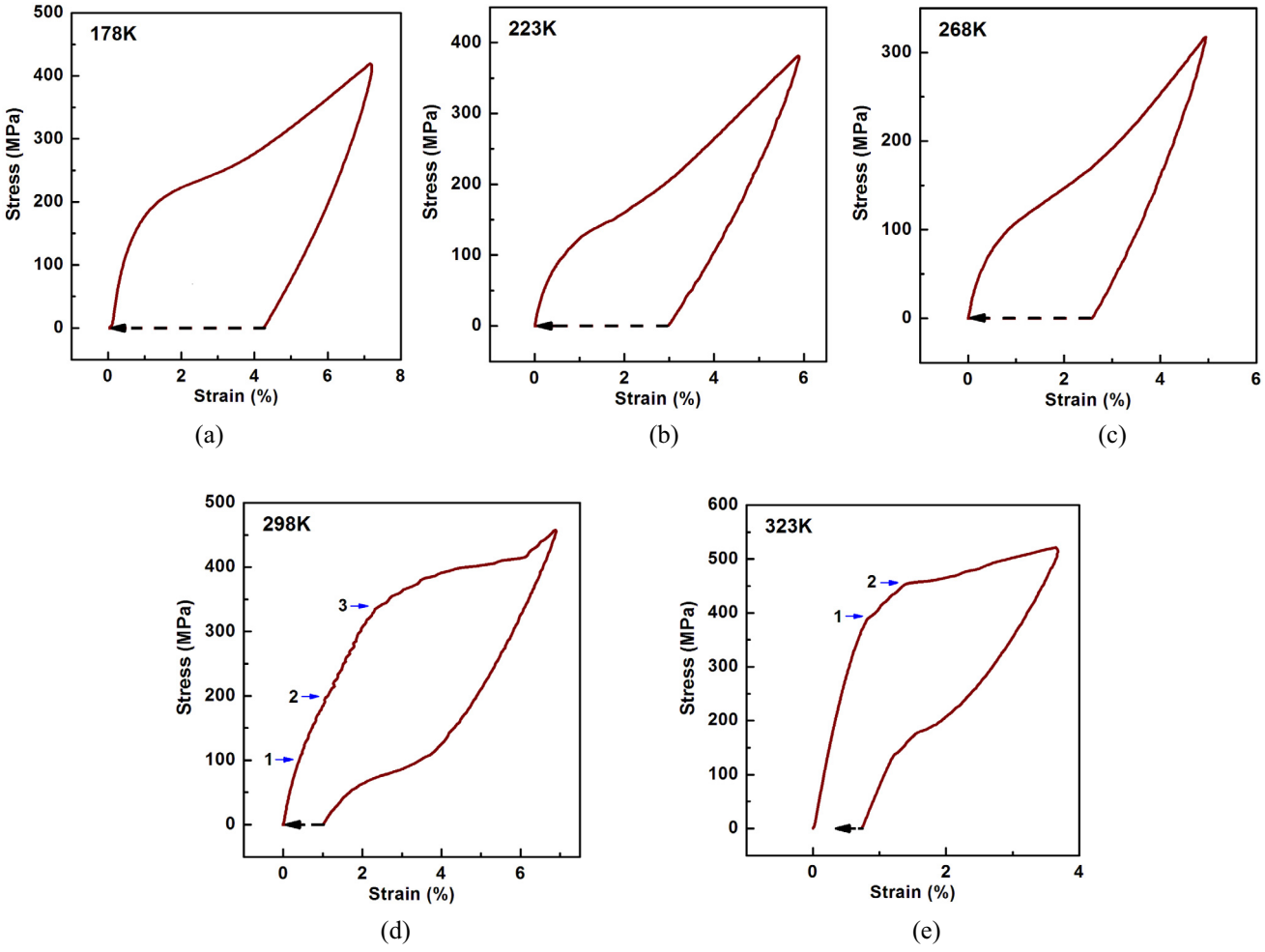

Fig. 10. Tensile stress–strain curves (solid lines) of the sample aged at 773 K for 30 min under 70 MPa, measured during heating at (a) 178 K, (b) 223 K, (c) 268 K, (d) 298 K and (e) 323 K. The dashed arrows indicate the recovery of residual strain during heating to 393 K.

approach ensures that the target temperature for each test was reached during cooling from 393 K. For the tests during heating (Fig. 10), the sample was cooled to 153 K before each test and then heated to the target temperature for testing and, finally, the sample was heated to 393 K to examine the recovery of the residual strain (shown by the dashed arrows in Fig. 10). This ensures that each testing temperature was reached during heating from 153 K. For all the tests, the maximum applied load was carefully controlled to avoid permanent plastic deformation by dislocation slip. As demonstrated below, only the last test during heating involves some plastic deformation that cannot recover during subsequent heating; no further tests were performed after that.

Now, the stress–strain curves in Figs. 9 and 10 are interpreted with the help of the established phase diagram in Fig. 8. During cooling, the sample is in the pure austenitic state at 298 K (see Fig. 8). As can be seen from the stress–strain curve (Fig. 9a), there is a kink at ~170 MPa (arrow 1) and a stress plateau at ~350 MPa (arrow 2) during loading, which correspond to the stress-induced transformations from austenite to R phase (arrow 1) and from R phase to martensite (arrow 2), respectively. In contrast to the stress plateau corresponding to the transformation from R phase to martensite, there is no obvious stress plateau associated with the austenite to R phase transformation. This is probably because the stress-induced R-phase transformation is a gradual, stable process and the deformation during this transformation is homogeneous [40]. During unloading, most of the strain recovers, while a small amount of strain still remains. The strain recovery is attributed to the reverse transformation from martensite to austenite on unloading. However, at this temperature (which falls between A_s and A_f under zero stress), there still remains a small amount of stress-induced martensite that is thermodynamically stable (reasonably assuming that the precipitates do not evolve at the test temperature and within the experimental time scale) after unloading, as indicated from the phase diagram in Fig. 8 (the heating process along the direction of the horizontal dashed arrow should be referred to; for consistency, the unloading process is also indicated by a vertical dashed arrow); this accounts for the small amount of unrecoverable strain after unloading. Upon heating, the residual strain recovers fully (as indicated by the dashed arrow in Fig. 9a) as the thermodynamically stable martensite transforms back to austenite. No permanent plastic deformation is observed.

Further cooling to 288 K leads to the coexistence of R phase and austenite (see Fig. 8). The stress–strain curve at this temperature (Fig. 9b) shows two kinks (arrows 1 and 2, arrow 2 being less obvious) and a stress plateau (at ~310 MPa, arrow 3) on loading. With reference to Fig. 8, these features correspond to the following processes: (1) reorientation of the R phase R1 (arrow 1) (R1 is used to distinguish it from the stress-induced R phase from the coexisting austenite, R2) and subsequent stress-induced transformation from R1 to martensite (arrow 3), and (2) stress-induced transformations first from austenite to R2 (arrow 2) and then from R2 to martensite (arrow 3). Upon unloading, a minor part of the strain recovers as

part of the martensite transforms back to austenite; however, a major part of the strain remains unrecoverable, because a large amount of martensite is thermodynamically stable after unloading at this temperature (between A_s and A_f) (see Fig. 8). During heating, all the residual strain recovers as a result of the transformation from the thermodynamically stable martensite to austenite.

After cooling to 268 K, the sample is in the pure R phase state (Fig. 8). Two obvious stress plateaus, one at ~50 MPa (arrow 1) and the other at ~250 MPa (arrow 2), can be observed during loading (see Fig. 9c). The first plateau (arrow 1) corresponds to the R-phase reorientation, and the second (arrow 2) corresponds to the stress-induced transformation from R phase to martensite. A similar phenomenon, termed "two-stage yielding", was observed in Refs. [40,41]. Actually, this type of "yielding" is different from the yielding as a result of plastic deformation by dislocation slip (e.g. that in Fig. 6a), because the residual strain associated with this type of "yielding" can recover on subsequent unloading and/or heating. During unloading (Fig. 9c), all the strain remains unrecoverable, because the stress-induced martensite is thermodynamically stable at this temperature (below A_s) (see Fig. 8). Upon heating, full recovery of the residual strain occurs with the thermodynamically stable martensite transforming to austenite.

At 223 K reached during cooling, martensite and R phase coexist in the sample (Fig. 8). The stress–strain curve at this temperature exhibits distinct "wavy" characteristics between 35 MPa and 100 MPa (indicated by arrows in the magnified view in the inset of Fig. 9d) during loading, but no clearly separated stress plateaus can be distinguished. The following processes are expected to occur during loading: (1) reorientation of the martensite M1 (M1 is used to distinguish it from the stress-induced martensite transformed from the coexisting R phase, M2), and (2) reorientation of the R phase and subsequent stress-induced transformation from R phase to martensite M2. However, at this temperature the critical stresses for martensite reorientation, R phase reorientation, and stress-induced transformation from R phase to martensite are all relatively low and close to each other; thus, the stress plateaus associated with these processes cannot be separated and, instead, the distinct "wavy" characteristics appear (Fig. 9d). Upon unloading, no strain recovery can be observed as the martensite reorientation is irreversible and the stress-induced martensite from the R phase is thermodynamically stable at this temperature (see Fig. 8). Upon heating to 393 K, the residual strain recovers fully as both the reoriented martensite M1 and the thermodynamically stable stress-induced martensite M2 transform to austenite.

Further cooling to 178 K results in a pure martensitic state (Fig. 8). There is a stress plateau at ~200 MPa on the stress–strain curve during loading (Fig. 9e), which corresponds to the martensite reorientation. Upon unloading, the strain does not recover, owing to the irreversibility of the martensite reorientation process. Upon heating to 393 K, there is a full recovery of the residual strain with the martensite transforming to austenite. It is seen from Fig. 9 that the stress plateau (corresponding to either transformation from R phase to martensite or martensite reorientation) in the stress–strain curves first decreases and then increases with increasing temperature; this is because: (i) at temperatures above the martensitic transformation temperature, higher stress is required for stress-induced transformation if the test temperature is higher (according to the Clausius–Clapeyron relation); and (ii) at temperatures below the martensitic transformation start temperature, higher stress is needed to move the twin boundaries if the test temperature is lower, as the twin boundaries are more mobile around transformation temperatures. Correspondingly, the maximum applied stress for each stress–strain test, which was carefully controlled so that all the characteristic features can be observed and meanwhile no permanent plastic deformation by slip occurs, shows the same general trend with varying temperature.

During heating, measurements were performed at 178, 223, 268, 298 and 323 K (Fig. 10). As can be seen, although the testing temperatures are the same, the stress–strain curves are quite different depending on whether these testing temperatures are reached during cooling or during heating (compare Fig. 10b with Fig. 9d (223 K), Fig. 10c with Fig. 9c (268 K), and Fig. 10d with Fig. 9a (298 K)). This clearly demonstrates the thermal history dependence of the stress–strain behaviour. The origin of this dependence lies in that the initial phases before loading are different, even if the temperatures are the same, depending on the thermal history. At all the temperatures of 178, 223 and 268 K during heating (Fig. 10a–c), the sample is fully martensitic (as indicated from Fig. 8), and shows qualitatively the same stress–strain behaviour as that at 178 K reached during cooling (Fig. 9e).

After heating to 298 K, austenite and martensite coexist (see Fig. 8). During loading, two kinks and a stress plateau appear (Fig. 10d), corresponding to (1) reorientation of the martensite M1 (arrow 1), and (2) stress-induced transformations, first from austenite to R phase (arrow 2) and then to martensite M2 (arrow 3). After unloading, a major part of the strain recovers as part of the martensite transforms back to austenite; however, a minor part of the strain still remains unrecoverable, because part of martensite is thermodynamically stable after unloading at this temperature (between A_s and A_f). Upon heating, all the residual strain recovers with martensite transforming to austenite.

Further heating to 323 K leads to the pure austenitic state. The stress–strain curve (Fig. 10e) exhibits a kink and a stress plateau during loading, corresponding to the stress-induced transformations from austenite to R phase (arrow 1) and from R phase to martensite (arrow 2), respectively. During unloading, about half the strain recovers, while the other half remains unrecoverable. Upon heating, part of the residual strain recovers, but the other part is still unrecoverable. It should be noted that, at 323 K (above A_f), the stress-induced martensite is thermodynamically unstable, as indicated from Fig. 8. Nevertheless, owing to the high critical stress for stress-induced transformations at this temperature, localized plastic deformation by slip occurs during the stress-induced transformations and part of the stress-induced martensite is stabilized by dislocation strain fields [21,37–39], while the other part of martensite can still transform back to austenite, which accounts for the recoverable strain, during unloading; the permanent plastic deformation and the stabilization of martensite account for the unrecoverable strain after unloading. Upon heating, the stabilized martensite transforms back to austenite, leading to the recovery of the residual strain; the unrecoverable residual strain is attributed to the permanent plastic deformation by slip. Considering the occurrence of permanent plastic deformation, no further tests were performed.

From Figs. 10e and 8, one can see that the critical stresses at 323 K for the stress-induced transformations from austenite to R phase and from R phase to martensite are close to each other. According to the phase diagram in Fig. 8, if one tests the sample at an even higher temperature, e.g. 340 K, there will be a stress-induced transformation directly from austenite to martensite without passing through the intermediate R phase, because at this temperature the critical stress for stress-induced transformation from austenite to R phase is higher than that for transformation from austenite to martensite; but in that case, the austenite may already completely yield (owing to permanent plastic deformation) before reaching the high critical stress needed for stress-induced transformation from austenite to martensite.

As demonstrated above, the present authors investigated in detail the temperature- and thermal-history-dependent stress–strain behaviour in different phase regions during both cooling and heating, and established a stress–temperature phase diagram to help explicitly interpret the thermomechanical behaviour in

Please cite this article in press as: Cong DY et al. Thermomechanical properties of Ni–Ti shape memory wires containing nanoscale precipitates induced by stress-assisted ageing. Acta Biomater (2014), http://dx.doi.org/10.1016/j.actbio.2014.08.017

the precipitate-containing Ni–Ti alloys. The comprehensive information obtained from this study is indeed very instructive for designing functionalities for biomedical applications in different temperature regions in SMAs.

3.4. Effect of ageing on low-temperature mechanical behaviour of martensite

To investigate the effect of ageing on martensite reorientation, the stress–strain curves of the samples aged at 773 K under 70 MPa for different time periods were measured at a low temperature of 133 K, which is well below the martensitic transformation temperatures of these samples. For each measurement, the sample was first heated to 393 K and then cooled to 133 K for testing and, after testing, the sample was heated again to 393 K to examine the recovery of the residual strain (after unloading) on heating. Fig. 11a shows the stress–strain curves at 133 K for the samples aged for 10, 15, 20, 30, 60 and 120 min, as well as that for the solution-treated sample. As can be seen, there is a stress plateau during loading on each stress–strain curve, which corresponds to the martensite reorientation via twin boundary movement. Upon unloading, the strain cannot recover, because the martensite reorientation process is irreversible. Upon heating, the residual strain almost fully recovers (for clarity, not shown in the figure) with martensite transforming to austenite. It is seen that the length of the stress plateau (the strain as a result of martensite reorientation) of the solution-treated sample is larger than that of the aged samples, as precipitation in the aged samples leads to the reduction in the amount of Ni–Ti matrix.

It is clear from Fig. 11a that the stress plateau corresponding to martensite reorientation becomes higher with prolonged ageing time. As the stress–strain curve for martensite deviates from linearity from very low stress levels during loading (Fig. 11a and Refs. [42,43]), for convenience, the critical stress for martensite reorientation (denoted as σ_{cr}) is estimated as the stress at 2% strain (2% strain is at the beginning of the steady stress plateau) (as indicated by the dashed arrow in Fig. 11a). Fig. 11b shows the critical stress for martensite reorientation (σ_{cr}) at 133 K as a function of ageing time. Clearly, σ_{cr} increases monotonically with prolonged ageing time; it first increases rapidly with ageing time increasing up to 30 min, and then increases relatively slowly as ageing time increases further to 120 min. There is a considerable increase of

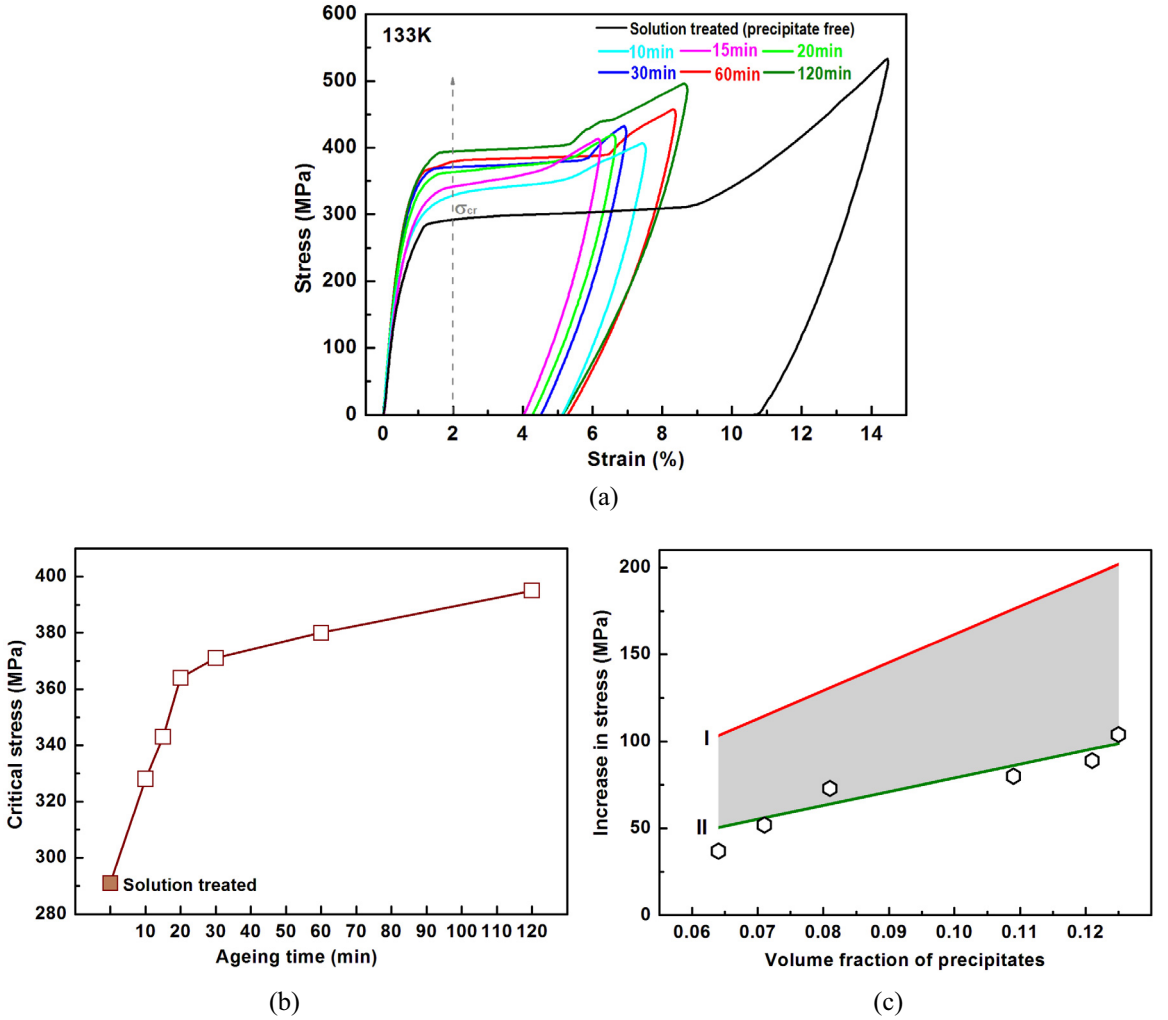

Fig. 11. (a) Tensile stress–strain curves at 133 K for the samples aged at 773 K for 10, 15, 20, 30, 60 and 120 min under 70 MPa. A dashed arrow, pointing in the direction of increasing ageing time, is placed at 2% strain to assist in estimating the critical stress for martensite reorientation. (b) Critical stress for martensite reorientation at 133 K as a function of ageing time. The data for the solution-treated sample are also included in (a) and (b). (c) Experimental data (open symbols) for increase in critical stress for martensite reorientation and the calculated increase in applied stress to overcome the back stress for the cases with discs parallel to tensile axis (line I) and discs on cube planes (line II) as a function of volume fraction of precipitates.

Please cite this article in press as: Cong DY et al. Thermomechanical properties of Ni–Ti shape memory wires containing nanoscale precipitates induced by stress-assisted ageing. Acta Biomater (2014), http://dx.doi.org/10.1016/j.actbio.2014.08.017

104 MPa in σ_{cr} when comparing the σ_{cr} value for the sample aged for 120 min (395 MPa) with that for the solution-treated sample (291 MPa). This considerable increase in σ_{cr} is attributed to the strong interactions between precipitates (developed by stress-assisted ageing) and twin boundaries during martensite reorientation, which occurs via the movement of twin boundaries [6]. The underlying mechanisms responsible for such interactions are discussed in Section 4.3.

4. Discussion

4.1. Ni_4Ti_3 precipitates in Ni-rich Ni–Ti alloys

Homogeneously distributed nanoscale precipitates were developed by stress-assisted ageing in slightly Ni-rich Ni–Ti wires in the present study. In Ni-rich Ni–Ti alloys, Ni_4Ti_3 precipitates occur in the B2 austenite matrix after appropriate heat treatments. These precipitates have an ordered rhombohedral crystal structure with $a = 0.670$ nm and $\alpha = 113.9°$ [44], or $a = b = 1.124$ nm and $c = 0.508$ nm in the hexagonal description [45]. The orientation relationship between the Ni_4Ti_3 precipitate in the hexagonal (H) description and the B2 matrix (with $a = 0.301$ nm [46]) is: $(111)_{B2}//(001)_H$, $[3\bar{2}\bar{1}]_{B2}//[100]_H$ [44,45]; in this case, the $[111]_{B2}$ direction corresponds to the normal of the central plane of the lenticular precipitate [45]. Consequently, there can be eight precipitate variants forming on the four $\{111\}_{B2}$ planes; each two variants share the same $\{111\}_{B2}$ plane and are crystallographically twin related [44], so the eight variants can be grouped into four families (see Fig. 4 of Ref. [47]). Normally, only four different orientations can be distinguished by conventional SEM [48], each corresponding to one family of precipitates.

In an earlier study, all four possible families of precipitates were observed in a conventionally aged Ni–Ti alloy [26]. However, in the present study, only one or two families of Ni_4Ti_3 precipitates can be observed in the samples subjected to stress-assisted ageing, as shown in Figs. 1 and 2. This is because the formation of coherent Ni_4Ti_3 precipitates results in coherency stress fields and the external stress applied during ageing favours certain precipitate variants [24,46]; consequently, there are fewer precipitate variants forming during stress-assisted ageing than during conventional ageing.

4.2. Effect of precipitates on martensitic transformation temperatures

The martensitic and reverse transformation temperatures (M_p and A_p) of the aged samples increase monotonically with increasing ageing time (Figs. 4 and 5), which is attributed mainly to the formation of precipitates induced by stress-assisted ageing. This finding is in good agreement with the quite recent finite element simulation result that precipitation as a result of ageing shifts the phase transformation temperatures to higher values [49]. There have actually been many investigations on the effect of ageing on martensitic transformations [24–26]; nevertheless, the underlying mechanisms responsible for this effect are still not well understood. Most investigations attribute the effect of ageing on transformation temperatures to the Ni depletion in the matrix as a result of precipitate formation, and other factors are seldom considered. However, as discussed below, besides change in matrix composition, contributions from other factors also play an important role in affecting martensitic transformation temperatures.

The martensitic transformation temperature of Ni–Ti alloys is known to be very sensitive to their chemical composition [6,50,51]. As the Ni concentration of Ni_4Ti_3 precipitates c_P (57.14 at.%) is higher than that of the supersaturated matrix c_0 (50.73 at.%), the formation of precipitates results in depletion of Ni in the matrix. After the formation of precipitates with volume fraction V_f, the average Ni concentration of the matrix (c_{Ni}) becomes

$$c_{Ni} = \frac{c_0 - V_f c_P}{1 - V_f} \quad (1)$$

To find the correlation between composition and martensitic transformation temperatures, the experimental data of M_s and c_0 for solution-treated Ni–Ti alloys published in the literature [41,51–59] (open circles) and obtained in the present study (filled square) are shown in Fig. 12a. Solution-treated alloys are selected because they are precipitate-free and their overall composition reflects the actual composition in the matrix, i.e. $c_{Ni} = c_0$ (for the aged alloys reported in the literature, the actual matrix composition cannot be obtained from the published data therein). With an approach similar to that used in Ref. [24], a fourth-degree polynomial fit of the experimental data (M_s and $x = 100c_{Ni}$) shown in Fig. 12a was performed (the fourth degree is the lowest degree with which a reasonable fit can be obtained); the fitted results are shown in Fig. 12a as a solid line. As suggested by Khalil-Allafi et al. [24], the $M_p(x)$ curve can be obtained by shifting the fitted $M_s(x)$ curve down to the experimental M_p value of the solution-treated sample in the present study (filled square in Fig. 12a); the $M_p(x)$ curve obtained is plotted as a dashed line in Fig. 12a. However, the $M_p(x)$ data obtained above (Fig. 12a) are for the martensitic transformation from B2 austenite to B19′ martensite in solution-treated samples, which is different from the martensitic transformation from R phase to B19′ martensite in the samples subjected to stress-assisted ageing. Therefore, these $M_p(x)$ data cannot be compared directly with the experimental M_p values (shown in Fig. 5) for the aged samples in the present study. Instead, the focus is put on the austenitic transformation which, in both solution-treated and aged samples, is from B19′ martensite to B2 austenite; their A_p values are compared below.

According to Khalil-Allafi et al. [24], the A_p values can be estimated from the $M_p(x)$ data. As shown in Fig. 3, the difference between A_p and M_p of the solution-treated sample is 33 K. The$A_p(x)$ curve is created by correcting the $M_p(x)$ curve by this amount (33 K) and the $A_p(x)$ curve obtained is shown in Fig. 12b as a dashed line. Based on the experimental data from the aged samples in the present study, the actual Ni concentration of the matrix (c_{Ni}) in the aged samples is calculated according to Eq. (1), using the V_f values shown in Fig. 2d. The experimental A_p values (determined from the DSC curves in Fig. 4c) of the aged samples are shown as a function of c_{Ni} in Fig. 12b, with an enlarged view displayed in its inset. Clearly, both the calculated $A_p(x)$ curve and the dependence of experimental A_p on c_{Ni} show the same general trend: the transformation temperature increases with decreasing Ni concentration (corresponding to increasing ageing time and precipitate volume fraction). However, the magnitudes of the experimental data and the calculated values differ. The experimental A_p values of the aged samples are considerably lower than the values expected from the Ni depletion in the matrix as a result of precipitate formation; the difference amounts to as much as 45 K for the sample aged for 120 min. This clearly indicates that, besides matrix composition change, other factors also play an important role in affecting the martensitic transformation temperatures of the aged samples; these factors actually decrease the martensitic transformation temperatures while the depletion of Ni in the matrix raises them. The most probable factor is the coherency stress field induced by precipitation. This coherency stress field inhibits martensitic transformation (as it imposes a resistance to the lattice distortion produced by martensitic transformation) and promotes reverse transformation, resulting in a decrease in transformation temperatures [60,61]. Nevertheless, the effect of the coherency stress field is smaller compared with that of the depletion of Ni in the matrix, the competition of these

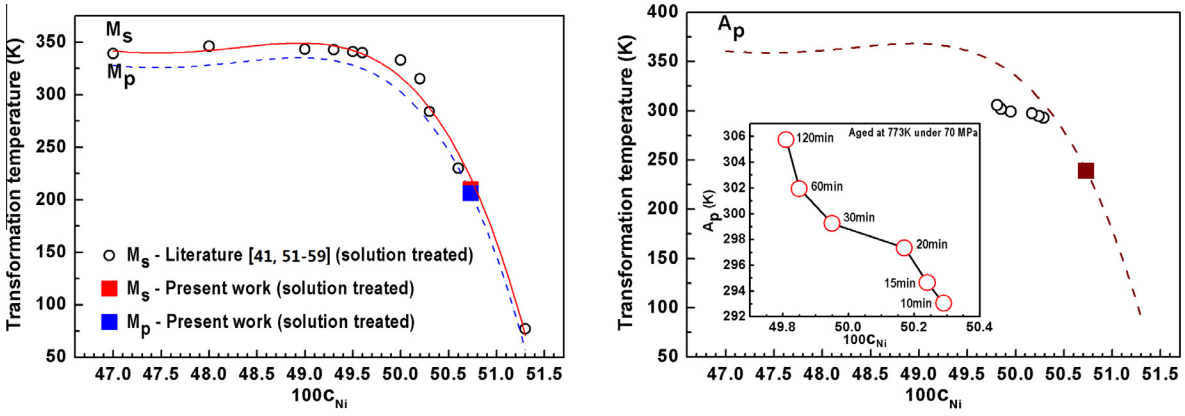

Fig. 12. (a) Martensitic transformation temperatures as a function of Ni concentration in solution-treated Ni–Ti alloys. The $M_s(x)$ ($x = 100c_{Ni}$) curve (solid line) is a fourth-degree polynomial fit of the experimental data published in Refs. [41,51–59] (open circles) and obtained in the present study (filled square). The $M_p(x)$ curve (dashed line) is obtained by shifting the $M_s(x)$ curve down to the experimental M_p value of the solution-treated sample in the present study (filled square). (b) $A_p(x)$ ($x = 100c_{Ni}$) curve (dashed line) estimated from the $M_p(x)$ data in (a) (the experimental A_p value of the solution-treated sample in the present study is shown as a filled square on this curve), and the experimental A_p values of the aged samples in the present study (open circles) shown as a function of Ni concentration in the matrix (the inset demonstrates the enlarged view, with the ageing time displayed beside the data points).

two factors resulting in the overall increase in martensitic transformation temperatures with increasing ageing time. Further investigations are needed to quantify to what extent the coherency stress field can affect the martensitic transformation temperatures.

4.3. Effect of precipitates on twin boundary movement

As is well known, precipitation strengthening is an important strengthening mechanism in metals and alloys. Over the past several decades, there have been extensive investigations on the interactions between precipitates and dislocations and their effect on mechanical properties in metals and alloys with dislocation slip as the deformation mode [62–65]. Nevertheless, there are fewer studies on the interactions between precipitates and twin boundaries during twin growth. The only available investigations on the effect of precipitates on twin growth are confined to deformation twins in, for example, Mg alloys [66,67]. To the best of the present authors' knowledge, there have been no investigations on the mechanisms for interactions between precipitates and twin boundaries during twin boundary movement in the case of transformation twins (formed as a result of martensitic transformation). Here, the mechanisms responsible for such interactions are discussed, based on the effect of ageing on the critical stress for martensite reorientation via twin boundary movement, which was examined in Section 3.4.

It is acknowledged that twin boundary movement involves the nucleation and glide of twinning dislocations, which are partial dislocations characterized by a step in the twin interface and a small Burgers vector, across the twinning plane [66,68]. Considering that the Ni_4Ti_3 precipitates are harder than the B2 austenite [69] and the martensite [70], it is reasonable to assume that the twinning partial dislocations bypass the precipitates leaving them unsheared. In this sense, Orowan strengthening is one possible mechanism for the interactions between precipitates and twin boundaries during twin boundary movement, which give rise to the increase in required critical stress (σ_{cr}). The Orowan stress required for the twinning dislocations to bow around the precipitates, also the increase in critical resolved shear stress (CRSS), can be estimated as [71]

$$\Delta\tau = \frac{Gb_T}{\lambda} \tag{2}$$

where G is the shear modulus of the matrix, b_T is the magnitude of the Burgers vector for twinning dislocations, and λ is the inter-precipitate spacing.

The shear modulus of the martensite matrix G is estimated from its Young's modulus E, according to $G = E/2(1+\nu)$ (ν is the Poisson's ratio). The macroscopic Young's modulus E of martensite in Ni–Ti was reported to be 20–50 GPa [72] and, here, the mean value of 35 GPa is taken. The Poisson's ratio ν was reported to be 0.35 [43,73]. Based on these values, G is estimated to be 13 GPa.

According to Christian and Mahajan [74], the magnitude of the Burgers vector for the elementary twinning dislocations can be calculated as $b_T = ds$, where d is interplanar spacing of the twinning plane $\mathbf{K_1}$, and s is the magnitude of twinning shear. In Ni–Ti, the <011> type II twinning is the most commonly observed twinning mode, with $\mathbf{K_1}$=(0.7205 1 $\bar{1}$) and s = 0.28040 [75,76]. The interplanar spacing of $\mathbf{K_1}$ is calculated with the lattice parameters of martensite, a = 0.2885 nm, b = 0.4120 nm, c = 0.4622 nm and β = 96.8° [77], to be d = 0.25645 nm, according to

$$\frac{1}{d^2} = \frac{1}{\sin^2\beta}\left(\frac{h^2}{a^2} + \frac{k^2\sin^2\beta}{b^2} + \frac{l^2}{c^2} - \frac{2hl\cos\beta}{ac}\right) \tag{3}$$

where h, k and l are the Miller indices of the crystallographic plane. Based on the values of s and d, b_T is calculated to be 0.0719 nm.

In accordance with Fig. 2c, an inter-precipitate spacing λ of ~100 nm was taken for the sample aged at 773 K under 70 MPa for 120 min. Substituting the above values of G, b_T and λ into Eq. (2) yields a $\Delta\tau$ value of 9.3 MPa. Assuming a Taylor factor of 3, the increase in critical stress for twin boundary movement (σ_{cr}) is calculated to be ~28 MPa. Apparently, this is significantly lower than the experimental value of 104 MPa (difference between the σ_{cr} values for the sample aged for 120 min and for the solution-treated sample, as presented in Section 3.4). Therefore, the Orowan strengthening model of twinning dislocations is insufficient to account for the increase in critical stress for twin boundary movement resulting from the presence of precipitates. Other factors should be considered.

As discussed below, back stress generation is likely to be the mechanism for the interactions between precipitates and twin boundaries during twin boundary movement. As the shear modulus G of the Ni_4Ti_3 precipitates (39 GPa) [12] is higher than that of martensite (13 GPa, as calculated above), the Ni_4Ti_3 precipitates

are stiffer than martensite. Thus, it is reasonable to assume that the precipitates are only elastically deformed during twin boundary movement. Since the material is deformed by simple shear during twin boundary movement, application of the twinning shear alone will result in a plastic strain discontinuity at the precipitate–matrix interface when the precipitates remain unsheared [66]. In order to moderate this strain discontinuity to produce a continuous strain field, a uniform mean stress in the matrix that opposes the stress causing plastic deformation, which is called back stress, is generated by the rigid elastically deforming precipitates [66,71,78,79]. This back stress must be overcome by the applied stress to continue deformation. For matrix and precipitates with different shear modulus, provided that there is no plastic relaxation, the back stress is given by [78]

$$\tau = 2\gamma D G_m V_f \varepsilon_p \quad (4)$$

where γ is the accommodation factor, G_m is the shear modulus of the martensite matrix, V_f is the volume fraction of precipitates, ε_p is the amount of tensile plastic strain, and D is the modulus correction factor.

The disc-like shape of precipitates is used for back stress estimation. Taking into account the images taken on the cross section of the wire samples (Fig. 2), the case with discs parallel to the tensile axis is first considered, which yields the upper extreme of the predicted back stress. In this case, γ is taken to be ¾ according to Ref. [78], and D is estimated to be 3, with $D = G_p/G_m$ (G_p and G_m are the shear moduli of precipitate and martensite matrix, respectively; G_p = 39 GPa and G_m = 13 GPa, as mentioned earlier) [78]. For the sample aged at 773 K under 70 MPa for 120 min, V_f is 0.125, as given in Fig. 2d. The amount of plastic strain ε_p at 2% strain, at which the critical stress for martensite reorientation is determined, is estimated to be 1.38% (the total strain, 2%, subtracted by the elastic portion) for the sample aged for 120 min (note that this plastic strain can recover on heating). Substituting the above values of γ, D, G_m, V_f and ε_p into Eq. (4) yields a τ value of 101 MPa. Using the Tresca criterion as the yield criterion [78], the increase in applied stress to continue deformation is $\Delta\sigma = 2\tau$=202 MPa for the sample aged for 120 min.

Then, the case with discs on cube planes is considered, which leads to the lower extreme of the predicted back stress. In this case γ is estimated, with $\gamma = (2-\nu)/4(1-\nu)$ [78], to be 0.635, and D is estimated to be 1.734, according to the following relation for discs on cube planes [78]

$$D = \frac{G_p}{G_p - \gamma(G_p - G_m)} \quad (5)$$

Substituting the values of γ, D, G_m, V_f and ε_p for the sample aged for 120 min into Eq. (4) yields a τ value of 49 MPa. With the Tresca criterion, $\Delta\sigma$ is estimated as 2τ=98 MPa. The increase in applied stress to overcome the back stress for further deformation should be between the two extremes, i.e. in the range 98–202 MPa for the sample aged for 120 min. This is on the same order of the experimental value of 104 MPa (increase in σ_{cr} when comparing the sample aged for 120 min and the solution-treated sample).

Fig. 11c shows the increase in applied stress calculated for the cases with discs parallel to tensile axis (line I) and discs on cube planes (line II) as a function of V_f, as well as the experimental data (open symbols) for all the aged samples. The predicted increase in applied stress that is needed to overcome the back stress should, in principle, lie between line I and line II. Clearly, the predicted values and the experimental data have the same order of magnitude. Nevertheless, the predicted values are in general larger than the experimental ones, which might indicate the occurrence of local plastic relaxation (by dislocation slip) at the matrix–precipitate interface. In principle, the resulting plastic deformation is unrecoverable on heating, but the extent of plastic relaxation may be so trivial that it does not inhibit the full recovery of residual strain on heating, as observed experimentally. Based on the above discussion, it becomes clear that the back stress generation is the predominant mechanism for the interactions between precipitates and twin boundaries that give rise to the increase in critical stress for twin boundary movement.

5. Summary and conclusions

A high density of homogeneously distributed nanoscale Ni_4Ti_3 precipitates was developed during stress-assisted ageing at 773 K under 70 MPa in the slightly Ni-rich $Ni_{50.73}Ti_{49.27}$ shape memory wires. Both the size and volume fraction of precipitates increased with prolonged ageing time. The phase transformation behaviour and thermomechanical properties of these precipitate-containing samples were systematically investigated. All the samples subjected to stress-assisted ageing exhibited two-step transformations during cooling and a single step transformation during heating. Both the martensitic and reverse transformation temperatures increased monotonically as ageing time increased; but the R-phase transformation temperature did not depend strongly on ageing time.

The temperature- and thermal-history-dependent mechanical properties of the samples subjected to stress-assisted ageing were comprehensively examined. The underlying mechanisms responsible for the stress–strain behaviour in different phase regions both during cooling and during heating were elucidated with the help of the stress–temperature phase diagram established based on the strain–temperature behaviour under different applied stresses. The establishment of the phase diagram and the interpretation of the temperature-dependent stress–strain behaviour are indeed very instructive for designing SMAs with different functionalities for biomedical applications.

The effect of precipitates on twin boundary movement in the case of transformation twins was explored for the first time, and the underlying mechanism for this effect was elucidated. Mechanical testing at the very low temperature of 133 K revealed that the critical stress for twin boundary movement (σ_{cr}) increased with increasing ageing time. There was a considerable increase of 104 MPa in σ_{cr} when comparing the sample aged at 773 K for 120 min under 70 MPa with the solution-treated sample. This is attributed to the presence of precipitates. The Orowan strengthening model of twinning dislocations is insufficient to account for the increase in σ_{cr} resulting from the presence of precipitates. The back stress generation is the predominant mechanism for the interactions between precipitates and twin boundaries during twin boundary movement, which give rise to the increase in σ_{cr}. These results contribute to deepening the understanding of the deformation mechanisms of martensite in precipitation-strengthened SMAs and are useful for developing high-performance biomedical SMAs.

Acknowledgements

The project related to this work is supported by the National Natural Science Foundation of China (No. 11305008) and the National Basic Research Program of China (973 Program) under Contract No. 2012CB619405 and by Deakin University via the ADPRF scheme. Rob Pow is acknowledged for his assistance in laboratory work related to DMA experiments.

Appendix A. Figures with essential color discrimination

Certain figures in this article, particularly Figs. 1–12 are difficult to interpret in black and white. The full color images can be found in

the on-line version, at http://dx.doi.org/10.1016/j.actbio.2014.08.017.

References

[1] Otsuka K, Wayman CM, editors. Shape memory materials. Cambridge: Cambridge University Press; 1998.
[2] Baxevanis T, Parrinello AF, Lagoudas DC. On the fracture toughness enhancement due to stress-induced phase transformation in shape memory alloys. Int J Plast 2013;50:158–69.
[3] Chen Y, Zhang XX, Dunand DC, Schuh CA. Shape memory and superelasticity in polycrystalline Cu–Al–Ni microwires. Appl Phys Lett 2009;95:171906.
[4] Ma J, Karaman I, Noebe RD. High temperature shape memory alloys. Int Mater Rev 2010;55:257–315.
[5] Young ML, Wagner MFX, Frenzel J, Schmahl WW, Eggeler G. Phase volume fractions and strain measurements in an ultrafine-grained NiTi shape-memory alloy during tensile loading. Acta Mater 2010;58:2344–54.
[6] Otsuka K, Ren X. Physical metallurgy of Ti–Ni-based shape memory alloys. Prog Mater Sci 2005;50:511–678.
[7] Tanaka Y, Himuro Y, Kainuma R, Sutou Y, Omori T, Ishida K. Ferrous polycrystalline shape-memory alloy showing huge superelasticity. Science 2010;327:1488–90.
[8] Cong DY, Roth S, Schultz L. Magnetic properties and structural transformations in Ni–Co–Mn–Sn multifunctional alloys. Acta Mater 2012;60:5335–51.
[9] Daly S, Ravichandran G, Bhattacharya K. Stress-induced martensitic phase transformation in thin sheets of nitinol. Acta Mater 2007;55:3593–600.
[10] Hamilton RF, Sehitoglu H, Chumlyakov Y, Maier HJ. Stress dependence of the hysteresis in single crystal NiTi alloys. Acta Mater 2004;52:3383–402.
[11] Waitz T. The self-accommodated morphology of martensite in nanocrystalline NiTi shape memory alloys. Acta Mater 2005;53:2273–83.
[12] Wagner MFX, Windl W. Elastic anisotropy of Ni_4Ti_3 from first principles. Scripta Mater 2009;60:207–10.
[13] Delville R, Malard B, Pilch J, Sittner P, Schryvers D. Microstructure changes during non-conventional heat treatment of thin Ni–Ti wires by pulsed electric current studied by transmission electron microscopy. Acta Mater 2010;58:4503–15.
[14] Duerig T, Pelton A, Stöckel D. An overview of nitinol medical applications. Mater Sci Eng A 1999;273–275:149–60.
[15] Rondelli G. Corrosion resistance tests on NiTi shape memory alloy. Biomaterials 1996;17:2003–8.
[16] Bogdanski D, Köller M, Müller D, Muhr G, Bram M, Buchkremer HP, et al. Easy assessment of the biocompatibility of Ni–Ti alloys by in vitro cell culture experiments on a functionally graded Ni–NiTi–Ti material. Biomaterials 2002;23:4549–55.
[17] Biesiekierski A, Wang J, Gepreel M Abdel-Hady, Wen C. A new look at biomedical Ti-based shape memory alloys. Acta Biomater 2012;8:1661–9.
[18] Lin B, Gall K, Maier HJ, Waldron R. Structure and thermomechanical behavior of NiTiPt shape memory alloy wires. Acta Biomater 2009;5:257–67.
[19] Robertson SW, Ritchie RO. In vitro fatigue–crack growth and fracture toughness behavior of thin-walled superelastic Nitinol tube for endovascular stents: a basis for defining the effect of crack-like defects. Biomaterials 2007;28:700–9.
[20] Miyazaki S, Imai T, Igo Y, Otsuka K. Effect of cyclic deformation on the pseudoelasticity characteristics of Ti–Ni alloys. Metall Trans A 1986;17:115–20.
[21] Gall K, Maier HJ. Cyclic deformation mechanisms in precipitated NiTi shape memory alloys. Acta Mater 2002;50:4643–57.
[22] Sehitoglu H, Anderson R, Karaman I, Gall K, Chumlyakov Y. Cyclic deformation behavior of single crystal NiTi. Mater Sci Eng A 2001;314:67–74.
[23] Zhou N, Shen C, Wagner MFX, Eggeler G, Mills MJ, Wang Y. Effect of Ni_4Ti_3 precipitation on martensitic transformation in Ti–Ni. Acta Mater 2010;58:6685–94.
[24] Khalil-Allafi J, Dlouhy A, Eggeler G. Ni_4Ti_3-precipitation during aging of NiTi shape memory alloys and its influence on martensitic phase transformations. Acta Mater 2002;50:4255–74.
[25] Fan G, Chen W, Yang S, Zhu J, Ren X, Otsuka K. Origin of abnormal multi-stage martensitic transformation behavior in aged Ni-rich Ti–Ni shape memory alloys. Acta Mater 2004;52:4351–62.
[26] Michutta J, Somsen C, Yawny A, Dlouhy A, Eggeler G. Elementary martensitic transformation processes in Ni-rich NiTi single crystals with Ni_4Ti_3 precipitates. Acta Mater 2006;54:3525–42.
[27] Abbasi-Chianeh V, Khalil-Allafi J. Influence of applying external stress during aging on martensitic transformation and the superelastic behavior of a Ni-rich NiTi alloy. Mater Sci Eng A 2011;528:5060–5.
[28] Kim JI, Liu Y, Miyazaki S. Effect of nano-scaled precipitates on shape memory behavior of Ti–50.9 at.% Ni alloy. Acta Mater 2004;52:487–99.
[29] Bataillard L, Bidaux JE, Gotthardt R. Interaction between microstructure and multiple-step transformation in binary NiTi alloys using in situ transmission electron microscopy observations. Philos Mag A 1998;78:327–44.
[30] Kim JI, Miyazaki S. Effect of nano-scaled precipitates on shape memory behavior of Ti–50.9 at.% Ni alloy. Acta Mater 2005;53:4545–54.
[31] Jiang F, Liu Y, Yang H, Li L, Zheng Y. Effect of ageing treatment on the deformation behaviour of Ti–50.9 at.% Ni. Acta Mater 2009;57:4773–81.
[32] Elahinia MH, Hashemi M, Tabesh M, Bhaduri SB. Manufacturing and processing of NiTi implants: a review. Prog Mater Sci 2012;57:911–46.
[33] Serin K, Neuser RD, Eggeler G, Kamaraj M, Kolbe H, Heitkemper M. A quantitative metallographic study of rafting and gamma-channel widening during creep in single crystal nickel base super alloys. Pract Met 2001;38:680–98.
[34] Ke C, Ma X, Zhang X. Phase field simulation of growth kinetics of coherent Ni_4Ti_3 precipitate in NiTi shape memory alloy. Acta Metall Sinica 2010;46:84–90.
[35] Frick CP, Ortega AM, Tyber J, Maksound AEM, Maier HJ, Liu Y, et al. Thermal processing of polycrystalline NiTi shape memory alloys. Mater Sci Eng A 2005;405:34–49.
[36] Li DY, Wu XF, Ko T. The effect of stress on soft modes for the phase transformation in a Ti–Ni alloy II. Effects of ageing and thermal cycling on the phase transformation. Philos Mag A 1991;63:603–16.
[37] Delville R, Malard B, Pilch J, Sittner P, Schryvers D. Transmission electron microscopy investigation of dislocation slip during superelastic cycling of Ni–Ti wires. Int J Plast 2011;27:282–97.
[38] Frick CP, Clark BG, Schneider AS, Maaß R, Petegem SV, Swygenhoven HV. On the plasticity of small-scale nickel–titanium shape memory alloys. Scr Mater 2010;62:492–5.
[39] Norfleet DM, Sarosi PM, Manchiraju S, Wagner MFX, Uchic MD, Anderson PM, et al. Transformation-induced plasticity during pseudoelastic deformation in Ni–Ti microcrystals. Acta Mater 2009;57:3549–61.
[40] Ng KL, Sun QP. Stress-induced phase transformation and detwinning in NiTi polycrystalline shape memory alloy tubes. Mech Mater 2006;38:41–56.
[41] Miyazaki S, Otsuka K. Deformation and transition behavior associated with the R-phase in Ti–Ni alloys. Metall Trans A 1986;17:53–63.
[42] Qiu S, Clausen B, Padula Ii SA, Noebe RD, Vaidyanathan R. On elastic moduli and elastic anisotropy in polycrystalline martensitic NiTi. Acta Mater 2011;59:5055–66.
[43] Rajagopalan S, Little AL, Bourke MAM, Vaidyanathan R. Elastic modulus of shape-memory NiTi from in situ neutron diffraction during macroscopic loading, instrumented indentation, and extensometry. Appl Phys Lett 2005;86:081901.
[44] Tadaki T, Nakata Y, Shimizu K, Otsuka K. Crystal structure, composition and morphology of a precipitate in an aged Ti–51 at.% Ni shape memory alloy. Trans Jpn Inst Met 1986;27:731–40.
[45] Tirry W, Schryvers D. Quantitative determination of strain fields around Ni_4Ti_3 precipitates in NiTi. Acta Mater 2005;53:1041–9.
[46] Li DY, Chen LQ. Selective variant growth of coherent $Ti_{11}Ni_{14}$ precipitate in a TiNi alloy under applied stresses. Acta Mater 1997;45:471–9.
[47] Guo W, Steinbach I, Somsen C, Eggeler G. On the effect of superimposed external stresses on the nucleation and growth of Ni_4Ti_3 particles: a parametric phase field study. Acta Mater 2011;59:3287–96.
[48] Cao S, Nishida M, Schryvers D. Quantitative three-dimensional analysis of Ni_4Ti_3 precipitate morphology and distribution in polycrystalline Ni–Ti. Acta Mater 2011;59:1780–9.
[49] Baxevanis T, Cox A, Lagoudas DC. Micromechanics of precipitated near-equiatomic Ni–rich NiTi shape memory alloys. Acta Mech 2014;225:1167–85.
[50] Tang W, Sundman B, Sandström R, Qiu C. New modelling of the B2 phase and its associated martensitic transformation in the Ti–Ni system. Acta Mater 1999;47:3457–68.
[51] Frenzel J, George EP, Dlouhy A, Somsen C, Wagner MFX, Eggeler G. Influence of Ni on martensitic phase transformations in NiTi shape memory alloys. Acta Mater 2010;58:3444–58.
[52] Prokoshkin SD, Korotitskiy AV, Brailovski V, Turenne S, Khmelevskaya IY, Trubitsyna IB. On the lattice parameters of phases in binary Ti–Ni shape memory alloys. Acta Mater 2004;52:4479–92.
[53] Smith JF, Jiang Q, Luck R, Predel B. Cp and fractal phase transformation in the shape memory alloy Ni–52Ti. Mater Sci Eng A 1991;149:111–20.
[54] Zhang L, Xie C, Wu J. Martensitic transformation and shape memory effect of Ti–49 at.% Ni alloys. Mater Sci Eng A 2006;438–440:905–10.
[55] Balak Z, Abbasi SM. Influence of the Ti content, training cycles and pre-strain on the two-way shape memory effect in NiTi alloys. Mater Des 2011;32:3992–6.
[56] Tang W, Sandström R, Wei ZG, Miyazaki S. Experimental investigation and thermodynamic calculation of the Ti–Ni–Cu shape memory alloys. Metall Mater Trans A 2000;31:2423–30.
[57] Wasilewski RJ, Butler SR, Hanlon JE. On the martensitic transformation in TiNi. Met Sci J 1967;1:104–10.
[58] Nishiura T, Hayashi K, Nishida M. Electropolishing conditions for trace analysis of B19′ martensite in Ti–Ni shape memory alloys. Mater Sci Eng A 2008;481–482:446–51.
[59] Saburi T, Tatsumi T, Nemo S. Effects of heat-treatment on mechanical-behavior of Ti–Ni alloys. J Phys Colloques 1982;43:261–6.
[60] Zhang J, Cai W, Ren X, Otsuka K, Asai M. The nature of reversible change in M_s temperatures of Ti–Ni alloys with alternating aging. Mater Trans JIM 1999;40:1367–75.
[61] Chung CY, Chu CL, Wang SD. The effect of cyclic aging on the transformation temperatures of Ni-rich NiTi alloys. In: Pelton AR, Duerig T, editors. SMST-2003: proceedings of the international conference on shape memory and superelastic technologies. Menlo Park, CA: SMST Society; 2004. p. 129–34.
[62] Nicholson RB, Thomas G, Nutting J. The interaction of dislocations and precipitates. Acta Metall 1960;8:172–6.
[63] Ference T, Allen S. Dislocation/precipitate interactions during coarsening of a plastically strained high-misfit nickel-base superalloy. Metall Trans A 1986;17:2239–47.

Please cite this article in press as: Cong DY et al. Thermomechanical properties of Ni–Ti shape memory wires containing nanoscale precipitates induced by stress-assisted ageing. Acta Biomater (2014), http://dx.doi.org/10.1016/j.actbio.2014.08.017

[64] Clark BG, Robertson IM, Dougherty LM, Ahn DC, Sofronis P. High-temperature dislocation-precipitate interactions in Al alloys: an in situ transmission electron microscopy deformation study. J Mater Res 2005;20:1792–801.
[65] Terentyev D, Bonny G, Domain C, Pasianot RC. Interaction of a 1/2⟨1 1 1⟩ screw dislocation with Cr precipitates in bcc Fe studied by molecular dynamics. Phys Rev B 2010;81:214106.
[66] Robson JD, Stanford N, Barnett MR. Effect of precipitate shape on slip and twinning in magnesium alloys. Acta Mater 2011;59:1945–56.
[67] Stanford N, Geng J, Chun YB, Davies CHJ, Nie JF, Barnett MR. Effect of plate-shaped particle distributions on the deformation behaviour of magnesium alloy AZ91 in tension and compression. Acta Mater 2012;60:218–28.
[68] Müllner P, King AH. Deformation of hierarchically twinned martensite. Acta Mater 2010;58:5242–61.
[69] Young ML, Frotscher M, Bei HB, Simon T, George EP, Eggeler G. Nanoindentation of pseudoelastic NiTi containing Ni_4Ti_3 precipitates. Int J Mater Res 2012;103:1434–9.
[70] Wood AJM, Clyne TW. Measurement and modelling of the nanoindentation response of shape memory alloys. Acta Mater 2006;54:5607–15.
[71] Kelly A, Macmillan NH. Strong solids. Oxford: Clarendon Press; 1986.
[72] Wagner MFX, Windl W. Lattice stability, elastic constants and macroscopic moduli of NiTi martensites from first principles. Acta Mater 2008;56:6232–45.
[73] Dunand DC, Mari D, Bourke MAM, Roberts JA. NiTi and NiTi–TiC composites: Part IV. Neutron diffraction study of twinning and shape-memory recovery. Metall Mater Trans A 1996;27:2820–36.
[74] Christian JW, Mahajan S. Deformation twinning. Prog Mater Sci 1995;39:1–157.
[75] Matsumoto O, Miyazaki S, Otsuka K, Tamura H. Crystallography of martensitic transformation in Ti–Ni single crystals. Acta Metall 1987;35:2137–44.
[76] Zhang X, Sehitoglu H. Crystallography of the B2 → R → B19′ phase transformations in NiTi. Mater Sci Eng A 2004;374:292–302.
[77] Michal GM, Sinclair R. The structure of TiNi martensite. Acta Cryst B 1981;37:1803–7.
[78] Brown LM, Clarke DR. Work hardening due to internal stresses in composite materials. Acta Metall 1975;23:821–30.
[79] Brown LM, Stobbs WM. The work-hardening of copper-silica. I. A model based on internal stresses, with no plastic relaxation. Philos Mag 1971;23:1185–99.

Please cite this article in press as: Cong DY et al. Thermomechanical properties of Ni–Ti shape memory wires containing nanoscale precipitates induced by stress-assisted ageing. Acta Biomater (2014), http://dx.doi.org/10.1016/j.actbio.2014.08.017